Atmospheric Research 211 (2018) 38–51

Contents lists available at ScienceDirect

Atmospheric Research

journal homepage: www.elsevier.com/locate/atmosres

Analysis of rainfall time structures on a scale of hours

Miloslav Müller[a,b,*], Vojtěch Bližňák[a], Marek Kašpar[a]

[a] Institute of Atmospheric Physics CAS, Department of Meteorology, Bočni II 1401, Prague 4 141 31, Czech Republic
[b] Charles University, Faculty of Science, Department of Physical Geography and Geoecology, Albertov 6, Prague 2 128 43, Czech Republic

ARTICLE INFO

Keywords:
Rainfall time structure
Rainfall intensity
Weather radar
Half-time concentration index
Synthetic storm hyetograph

ABSTRACT

The paper is motivated by the enormous variability of short-term rainfall time structures which need to be discretized into several typical variants and explained from the viewpoint of rainfall types producing them. We present six variants of the time structure of 6-h rainfalls in Czechia, distinguished by a novel methodology for designing synthetic hyetographs. Reference 6-h rainfall episodes were extracted from radar-derived precipitation time series with a time resolution of 10 min, adjusted by daily data from rain gauges. The variants were distinguished by three indexes that quantify the precipitation concentration within time steps from one to six hours. The episodes with steady precipitation intensity during the entire episode are mainly stratiform or possibly mixed and frequently take much longer than six hours because of circulation patterns producing them; central and northeastern cyclonic types are most represented. All other variants of episodes frequently occur when a trough is situated above Central Europe. Episodes with steady intensity lasting about three hours are still mainly stratiform or mixed while two variants represented by "two-humped" hyetographs are usually mixed or convective. Two variants of most concentrated episodes are mainly convective or possibly mixed; they are characterized by enhanced frequency of southwestern and eastern cyclonic types. Future research on cluster frequencies among maximum precipitation episodes in various regions will enable the improvement of design hydrographs of small streams where runoff is basically influenced by the rainfall time structure.

1. Introduction

The effects of rainfall, such as flooding or landslides, mainly depend on precipitation amounts but also on rainfall distribution in space and time (Peleg et al., 2017). Thus, the performance of hydrological models strongly depends on the quality of precipitation data (Amengual et al., 2015; Dai et al., 2015). Locally, the effects of the same precipitation totals can be substantially enhanced or reduced because of differences in rainfall time structures (Guan et al., 2015). The main factors influencing the rainfall time structure are physical processes producing the precipitation. Generally, stratiform and convective precipitation can be recognized with respect to their lifting mechanisms. In midlatitudes, the first type is mainly produced by extratropical cyclones and/or atmospheric fronts connected with them; among them, it can be also produced or at least enhanced by upslope flows (Kunkel et al., 2012). Therefore, stratiform precipitation is usually wide-spread, steady, and long-lasting. On the contrary, convective precipitation is more localized and concentrated in time because of the dynamics of convective storms producing them (Leon et al., 2016). Nevertheless, both precipitation types can be combined because of convective storms nested into stratiform rain bands, or can follow one after another as it happens during the passage of a mesoscale convective system (Schiro and Neelin, 2018).

The differences between stratiform and convective precipitation have to be considered when designing curves representing the typical course of precipitation, called design storm hyetographs (Hailegeorgis and Alfredsen, 2017). Prodanovic and Simonovic (2004) presented three of the main approaches to designing storm hyetographs. The simplest approach uses only one point of the intensity-duration-frequency (IDF) curve and approximates the precipitation intensity course by a predefined geometrical shape. The simplest one – a rectangle – should represent purely stratiform rains while triangles (Ellouze et al., 2009) or even more complex shapes, such as the Desbordes hyetograph (Desbordes, 1978), can reflect also the attributes of convective rains. Alternatively, the design hyetograph can be constructed from all points of the IDF curve, as e.g., the Chicago hyetograph (Keifer and Chu, 1957), or can be directly obtained from rainfall records, as, e.g., four Soil Conservation Service design storms (Urban hydrology, 1986). The solutions substantially differ in the ratio between the maximum and the mean precipitation intensity, as well as in the runoff response (Alfieri et al., 2008).

Czechia is located within the fully humid temperate zone, with

* Corresponding author at: Institute of Atmospheric Physics CAS, Department of Meteorology, Bočni II 1401, Prague 4 141 31, Czech Republic.
E-mail addresses: muller@ufa.cas.cz (M. Müller), bliznak@ufa.cas.cz (V. Bližňák), kaspar@ufa.cas.cz (M. Kašpar).

https://doi.org/10.1016/j.atmosres.2018.04.015
Received 28 March 2017; Received in revised form 9 April 2018; Accepted 11 April 2018
Available online 24 May 2018

higher elevations belonging mainly to the boreal climate (Tolasz et al., 2007). Both the stratiform and the convective precipitation can produce extreme events there but their proportion strongly depends on the definition of extremes as well as on the topography of the region. If the definition is based on areal precipitation totals within large regions ($\sim 10^4$ km^2 or more) during at least one day, stratiform precipitation significantly prevails among extreme events in Czechia (Kašpar and Müller, 2008; Müller et al., 2015). Even at individual sites, stratiform events can prevail among daily precipitation maxima in Czechia, namely in mountains (Štekl et al., 2001). The shorter is the considered sub-daily time window, the higher is the percentage of convective events among the precipitation maxima, namely in lowlands (Šálek et al., 2012). Therefore, when Kulasová et al. (2004) designed synthetic hyetographs for Czechia, both their solutions reflected the differences in altitude. The so-called CHMU-hyetographs disaggregate the design 1-day precipitation total into hourly increments with respect to the percentage of the maximum design 1-h total, positioned into the 12th hour. The shapes of the hyetographs are very similar in the whole country; only the kurtosis makes a difference among hyetographs that represent locations with different topography, with mountain stations characterized by less-concentrated precipitation. Alternatively, four so-called UFA-hyetographs significantly differ among each other with respect to their shapes as they represent four regions that the country was divided into with respect to the precipitation climatology and altitude. The authors determined that the design 1-day rainfall was fully concentrated into six hours within two mainly lowland regions that covered more than 80% of the Czech territory because of the dominance of convective precipitation among precipitation maxima apart from mountain regions.

However, Fig. 1 demonstrates that individual regions can hardly be represented by only one design hyetograph each because of an enormous variability in the time structure of precipitation episodes even at the same altitude. We suggest that instead of dividing the country into several regions, the problem of rainfall design can be solved by constructing several synthetic hyetographs regardless the topography and quantifying their proportion throughout the country. This paper addresses the methodology, which (i) reduces the variability of the rainfall time structure by clustering reference precipitation episodes and (ii) enables the construction of synthetic storm hyetographs for individual clusters. Adjusted Czech radar precipitation data are applied because of their spatial coverage and high time resolution of 10 min. The clusters of detected precipitation episodes are further analyzed with respect to their relations to stratiform and convective rains to enable future explanation of regional distribution of the variants within the country. In this way, the procedure elucidates general patterns in precipitation behavior in the studied region. Finally, possible applications of the procedure are suggested in the conclusions.

2. Data and methods

To obtain reliable precipitation information at high spatial and temporal resolutions (Thorndahl et al., 2017), we applied radar-derived data combined with daily rain gauge measurements (Fig. 1), both covering warm parts (May–September) of the years 2002–2011 because high short-term precipitation intensities typically occur in these months in the Czech Republic (Bližňák et al., 2018). The original radar reflectivity data (Section 2.1) were first transformed into radar-only rainfall intensities (Section 2.2) and then adjusted by rainfall station data (Section 2.3). Finally, reference precipitation events were selected from the database (Section 2.4).

2.1. Original radar and rain gauge data

Radar reflectivity data were recorded by two Czech C-band Doppler radars (Brdy, Skalky) every 10 (2002–2008) and 5 (2009–2011) minutes and transformed into 1 km by 1 km square boxes. The spatial coverage includes the entire CR and the closest neighborhood (Novák, 2004). The composite product of the two radars was used which prefers the higher reflectivity values in pixels covered by both radars. Optimal locations of the radar sites (Fig. 1) cause that apart from very small border regions of the CR, the reflectivity products are not influenced by terrain blockage of the radar echo. The most distant pixels in the CR are located approximately 160 km from the nearest radar and the height of the lowest radar beam (0.1° elevation angle) is less than 2000 m above sea level for the large majority of pixels in the CR (Sokol and Bližňák, 2009). The Czech Hydrometeorological Institute (CHMI) manages both weather radars and carefully controls radar reflectivity products. The standard operational routines include checking by the Doppler filter to remove ground clutter and correction the vertical profiles of reflectivity (Novák and Kráčmar, 2002). In general, the quality of the Czech radar data is high and comparable to other data from European radar networks (Michelson et al., 2005).

Because the employed adjustment method (Section 2.3) requires rain gauge data at only daily resolution, measurements from the entire dense Czech weather station network could be utilized. The data were available from approximately 700 rain gauges for the study period (several times more than the number of automated rain gauges at that time). The daily rain gauge records were carefully checked by the CHMI before they were included in the database. Rain gauges recorded precipitation totals from 06 UTC to 06 UTC of the next day.

2.2. Radar-derived precipitation estimates

The basic radar product was 10-min radar-derived rain rates calculated in the following way. The interpolated reflectivity at 2 km above sea level (PseudoCAPPI 2 km) was converted into rain intensity. The altitude of this level overcomes the mountains at the state border by as much as several hundred meters (Fig. 1). For the most distant pixels from radar sites, the reflectivity from the lowest elevation 0.1° was used instead of linear interpolation between the adjacent beams. We used the standard Z–R relationship with respect to the Marshall-Palmer relationship between measured radar reflectivity and derived rain rates (Novák and Kráčmar, 2002) as it is the most common method to obtain precipitation information (e.g., Zhang et al., 2016). The main advantage of this approach is a straightforward relationship between measured reflectivity and derived precipitation. In addition, most of the *Z*-R relationships do not differ significantly for precipitation intensities between 20 and 200 mm/h (Rendon et al., 2013; Libertino et al., 2015). On the contrary, there are number of problems arising from the characteristics of both the radar and the precipitation and their detailed description can be found in many reviews (e.g., Villarini et al., 2014).

Subsequently, 10-min averages were calculated from neighboring values (two and three values from measurements with temporal resolutions of 10 and 5 min, respectively; in the latter case, the double weight was assigned to the term in the middle of the 10-min interval). If one of the values was missing, the average was not calculated and the 10-min interval was assigned a missing value.

The prepared 10-min radar-derived precipitation estimates were then accumulated from 06 UTC to 06 UTC of the next day to create daily radar-derived precipitation estimates that temporally matched daily rain gauge measurements. In total, 144 10-min radar integrations were summed together. If more than 18 integrations were missing, then the resulting daily radar-derived precipitation estimate was assigned a missing value. If the number of missing radar integrations was between 1 and 17, missing values were replaced by estimates based on linear interpolation between the adjacent preceding and subsequent 10-min radar integrations. Missing data were usually caused by the malfunction of one or both weather radars or by regular testing and checking of radar devices; such periods usually lasted from several hours to several days. On average, 94.3% of the days were covered by data, which is sufficient for the purposes of the study.

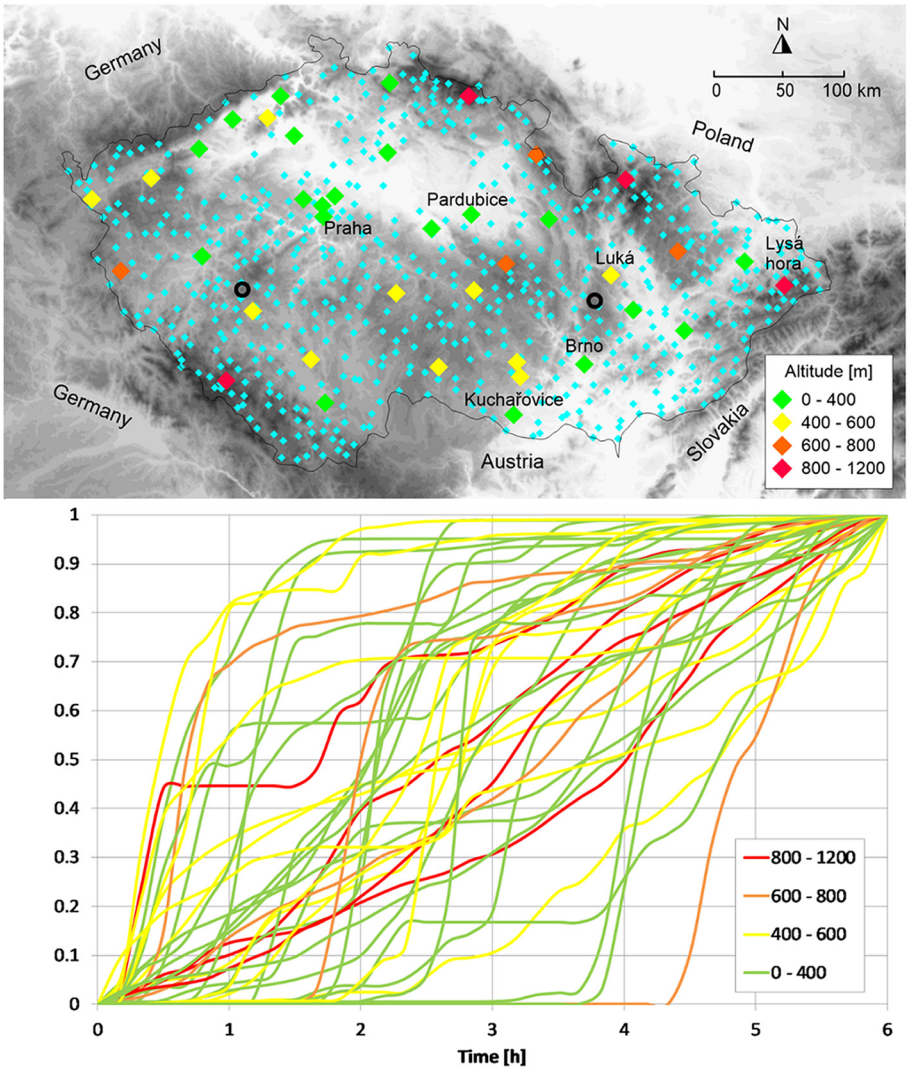

Fig. 1. Topography of the Czech Republic and normalized hyetographs of maximum 6-h precipitation episodes. The map depicts the positions of two Czech weather radars (circles), rain gauges used in the adjustment of radar data (small signs), and synoptic stations distinguished with respect to the mean altitude of the corresponding radar 1 by 1 km pixel (big signs; weather stations mentioned in Table 3 are highlighted). Normalized hyetographs of absolute 6-h precipitation maxima (2002 − 2011) in 39 respective pixels are expressed as cumulative percentage of 6-h rainfall.

2.3. Adjusted radar-based precipitation intensity

The applied adjustment method was based on the combination of 10-min radar-derived rain rates in 1 by 1 km pixels with daily precipitation totals measured by rain gauges. The method was developed by Sokol (2003) and later applied to hourly radar-derived precipitation estimates by Sokol and Bližňák (2009). The adjustment method consists of two steps.

First, the radar-derived rain field is generally adjusted to measurements from the rain gauges as a whole. For each day, the ratio p between the mean 1-day precipitation total calculated from all rain gauges and the mean 1-day precipitation total estimated from the corresponding radar pixels is determined using the formula

$$p = \frac{\sum_{k=1}^{n} G_k}{\sum_{k=1}^{n} R_k} \quad (1)$$

where G_k and R_k are the 1-day totals measured by a rain gauge and derived from the radar measurement in the pixel in which the rain gauge is located, respectively, and n is the number of all rain gauges in the domain. The ratio p is then used for the multiplication of radar-derived precipitation in every pixel of the radar domain between 0.3 and 3 (in which lower and higher values of p are replaced by 0.3 and 3, respectively). The limits prevent the corrected precipitation from achieving unrealistically low or high values. The aim of this procedure is to qualitatively equalize the whole radar-derived precipitation field based on the observed precipitation sum.

Second, the generally adjusted radar-derived rain rates are locally adjusted in individual pixels. For this purpose, every pixel in the radar domain is coupled with $n = 10$ nearest rain gauges. The gauges are assigned by a weight w proportional to the distance r [km] between the rain gauge and the considered pixel based on the equation

$$w = exp(-\alpha r) \quad (2)$$

where $\alpha = 0.1$. This value yielded the lowest Root-Mean-Square-Error when optimizing the interpolation method (Sokol, 2003). For each of the 10 gauges, the difference between G_k and R_k is weighted by w to get the constant q which is obtained by

$$q = \sum_{k=1}^{10} (G_k - R_k)\, w_k \quad (3)$$

The adjusted radar-derived 1-day precipitation estimates RA_{24h} are then calculated in each pixel using the following formula:

$$RA_{24h} = p\ RR_{24h} + q \quad (4)$$

where RR_{24h} is the 1-day radar-derived precipitation estimate. The Eq. (4) summarizes the effect of both applied parameters. While the parameter p multiplies the whole radar-derived precipitation field, the parameter q locally corrects precipitation estimates based on the nearby observations. Subsequently, the adjusted 1-day precipitation totals RA_{24h} are divided into 144 of 10-min precipitation totals RA_{10min} with respect to the 10-min radar-derived precipitation estimates RR_{10min} using the formula

$$RA_{10\,min} = RA_{24h}\ RR_{10\,min}/RR_{24h} \quad (5)$$

Using this method, we were able to obtain adjusted radar-derived 10-min precipitation estimates (hereafter called "10-min precipitation") for every pixel in the Czech Republic (over 78,000 pixels in total). See the paper by Bližňák et al. (2018) for an objective verification of the results and a comparison between adjusted radar-derived and rain-gauge precipitation intensities. For example, the absolute maximum 6-h total was recorded on 1 August 2002 in the pixel which the weather station Luká is located in (Fig. 1). Table 1 confirms a very good agreement between adjusted radar-based precipitation and hourly totals recorded by the rain gauge at the respective station.

2.4. Reference precipitation episodes

Based on the 10-min adjusted radar-based precipitation intensity data, we created their accumulations within moving time windows of various lengths. The processing resulted in data series of overlapping precipitation totals of 0.5, 1, 1.5, 2, 3, 6, 12, and 24 h, marked $R_{0.5}$, R_1, $R_{1.5}$, R_2, R_3, R_6, R_{12}, and R_{24}, respectively. The 6-h totals were selected as a basis value for characterizing a precipitation episode because the local effect of a rainstorm is mainly influenced by the short-term precipitation intensity and 6 h are sufficient to enable the analysis of the time structure of the episode using data with a temporal resolution of 10 min. Moreover, the 6-h duration corresponds to the so-called UFA-hyetographs designed by Kulasová et al. (2004), see Section 1. Unlike Manzato et al. (2016), we applied sliding totals to determine local maxima of R_6 within the data series. Each episode was further characterized by maximum R_{12} and R_{24} which the R_6 was nested in, as well as by the sequence of maximum R_3, $R_{1.5}$, R_1, and $R_{0.5}$ detected during the R_6, R_3, R_2, and R_1, respectively (Fig. 2).

Finally, it was necessary to extract a representative set of maximum precipitation episodes from the data. To ensure a high variability of the episodes, they were collected from 39 radar pixels where Czech synoptic weather stations are located because the stations are quite evenly distributed in terms of spatial coverage as well as altitude (Fig. 1). Moreover, validation of the employed adjusted radar-based precipitation intensity data was enabled by gauge-only data as well as the study of precipitation type was possible there using SYNOP reports (Section 2.6). In each of the 39 pixels, 50 independent maximum 6-h totals were selected from the 10-year period, which means that the episodes occurred once per month on average in each considered location. The total number of reference events was thus 1950. With respect to the local climatology, the events mostly had 6-h totals above 10 mm or even higher (especially in mountainous regions).

Table 1
Comparison between hourly precipitation totals measured by the rain gauge at the station Luká on 1 August 2002 (06–18 UTC) and corresponding adjusted radar-based estimates. Rain gauge data were excerpted from the SYNOP report where precipitation totals are rounded to full numbers.

Starting time [UTC]	06	07	08	09	10	11	12	13	14	15	16	17
Rain gauge totals [mm]	0	0	0	0	2	5	19	27	46	3	0	0
Radar-based totals [mm]	0.0	0.0	0.0	0.0	2.4	7.2	20.5	26.0	45.6	0.1	0.0	0.0

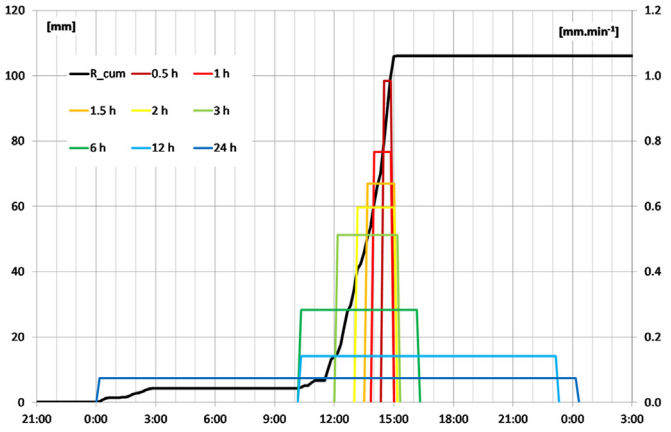

Fig. 2. Analysis of the highest 6-h precipitation total, recorded in anyone of 39 radar pixels corresponding to Czech synoptic weather stations during the study period 2002–2011 (station Luká, 1 August 2002). The black line expresses the accumulated precipitation total (R_cum, left axis); the color lines depict mean precipitation intensity during maximum 0.5, 1, 1.5, 2, 3, 6, 12, and 24 h (right axis).

For example, the analysis of the episode with absolute maximum R_6 is presented in Fig. 2. The maximum 6-h total R_6 = 101.9 mm was recorded from 10 a.m. but in fact, heavy rain fell only for 3.5 h between 11:30 a.m. and 3 p.m. As the result, the maximum R_3 = 92.1 was only 9.8 mm less than the maximum R_6. On the contrary, because the intensity changed only slightly during the 3 h, the maximum R_1 = 46.0 was significantly lower than the maximum R_3. The maximum R_{24} was 106.2 mm, only 4.3 mm more than the maximum R_6 on this day due to a previous weak precipitation episode after midnight.

2.5. Clustering of reference events by half-time concentration indexes

To distinguish variants of rainfall time structure, a novel methodology was proposed. The suggested tools are called half-time concentration indexes. They express the time concentration of 6-h rainfall in four time steps. In general, the indexes compare precipitation totals during gradually shortened time periods. The form is a normalized ratio between two precipitation totals within different time windows, the first one having a half-length than the second one.

The indexes are defined by the following formulas:

$$C_6 = 2(R_3/R_6 - 0.5) \quad (6)$$

$$C_{3,2} = \frac{2(R_{1.5}/R_3 - 0.5) + 2(R_1/R_2 - 0.5)}{2} = R_{1.5}/R_3 + R_1/R_2 - 1 \quad (7)$$

$$C_1 = 2(R_{0.5}/R_1 - 0.5) \quad (8)$$

The time windows used were basically selected as multiples of 1 h. The formula (7) combines two time steps to solve the problem that the result of splitting the 3-h time step in halves is not a whole-number multiple of 1.

Each of the indexes reaches values between 0 and 1 representing steady precipitation intensity and precipitation concentrated into one-half of the considered time step or less, respectively. Any 6-h precipitation total can thus be characterized by a triad of values C_6, $C_{3,2}$ and C_1 that can be considered as coordinates within a 3D diagram. The extremes of the diagram can be interpreted with respect to Table 2. Naturally, the real precipitation episodes regularly reach intermediate values. For example, the episode with absolute maximum R_6 (Fig. 2) reached the values of the half-time concentration indexes as follows:

Table 2
Coordinates of extremes of the 3D diagram presented in Fig. 5, with their interpretation.

[C_6; $C_{3,2}$; C_1]	Interpretation
1; 1; 1	100% of R_6 realized during 30 min or less
1; 1; 0	100% of R_6 realized during 1 h with uniform rainfall intensity
1; 0; 1	100% of R_6 realized in two separated episodes during 3 h
1; 0; 0	100% of R_6 realized during 3 h with steady rainfall intensity
0; 1; 1	R_6 divided into two identical episodes lasting 30 min or less; the interruption lasted at least 2 h
0; 1; 0	R_6 divided into two identical episodes lasting more than 30 but up to 60 min; the interruption lasted more than 2 h
0; 0; 1	*Not defined*
0; 0; 0	Steady rainfall intensity for at least 6 h

$$C_6 = 2(R_3/R_6 - 0.5) = 2(92.1/101.9 - 0.5) = 0.81$$

$$C_{3,2} = R_{1.5}/R_3 + R_1/R_2 - 1 = 60.3/92.1 + 46.0/71.6 - 1 = 0.30$$

$$C_1 = 2(R_{0.5}/R_1 - 0.5) = 2(92.1/101.9 - 0.5) = 0.28$$

The high value of C_6 corresponds to the fact that the episode was rather concentrated into three hours. Values of $C_{3,2}$ and C_1 are much lower because the precipitation intensity did not change very much during the three hours.

Because the half-time concentration indexes are independent of each other, they can be used to determine variants of the precipitation episodes. The set of precipitation episodes was partitioned by k-means clustering, which was preferred to hierarchical clustering because of the relatively large number of episodes and the lack of a clear hierarchy within the defined 3D space (Wilks, 2011) (see Table 2). The designed k-means clustering treated each episode as an object having a location in 3D space with the coordinates [C_6; $C_{3,2}$; C_1]. Each cluster in the partition is then determined by its member episodes and by its centroid for which the sum of distances from all episodes in that cluster is minimized. Eventually, based on tests using the silhouette technique, we applied a heuristic, the so-called k-means++ algorithm for cluster centroid initialization (Arthur and Vassilvitskii, 2007) and the squared Euclidean distance measure. For this setting, the mean silhouette values, which could be used as a clustering evaluation criterion (Kaufman and Rousseeuw, 1990), exceeded 0.5 for most of the considered k (see below), which indicated good consistency of the resulting clusters. The clustering procedure was performed repeatedly with step-by-step increasing numbers of distinguished clusters k. The clusters were labeled by codes cX_k, where X is a letter representing a cluster that is further transferred to analogous clusters in the next steps of clustering with respect to the similarity of the cluster coordinates [C_6; $C_{3,2}$; C_1].

2.6. Distinguishing between stratiform and convective precipitation

Because all 1950 reference episodes were selected from radar grid points where Czech synoptic weather stations are located (Section 2.4), it was possible to analyze the episodes also from the viewpoint of the predominant precipitation type by the suggested by Rulfová and Kyselý (2013). The method is based on weather state observations included in SYNOP reports during six consecutive hours. The following codes are considered to be typical for convective precipitation: 80–90 (showers), 91–99 (thunderstorms), 17–19, 25–27, and 29 (convective phenomena without precipitation at the station at the time of observation). Groups of codes typical for stratiform precipitation are 50–59 (drizzle), 60–79 (rain or alternatively snow not in the form of showers), and 20–24 (the same phenomena but without precipitation at the station at the time of observation).

Though only reports with manual observations could be considered, more than 63% of 1950 reference episodes were covered by the data. Three types of episodes were distinguished: convective, stratiform, and mixed. An episode was considered as convective (stratiform) if only convective (stratiform) phenomena were observed during the six hours; otherwise, the episode was labeled as mixed. The number of convective, mixed, and stratiform episodes was 409, 364, and 459, respectively. Rulfová and Kyselý (2013) applied additional criteria to reduce the number of episodes classified as mixed because of the further statistical analysis (Rulfová et al., 2016). Unlike them, we recognized the mixed episodes as an important category for our purposes. Therefore, no additional criteria were applied to reduce the number of such episodes.

For example, only one weather state code was reported during the episode with absolute maximum R_6 on 1 August 2002 at the station Luká, namely the code 95 (light to moderate thunderstorm). It was reported from 11 a.m. to 15 p.m. According to the algorithm, the episode was labeled as convective.

2.7. Analysis of circulation patterns during reference episodes

Reference episodes distinguished from the viewpoint of precipitation types were further analyzed with respect to circulation conditions producing them. The subjective classification operated by the CHMI was used for these purposes because of its focus on weather phenomena in the Czech territory. The catalogue containing 28 types was suggested by Brádka et al. (1961). The calendar of types is actualized every year on the web site of the weather service (http://portal.chmi.cz/historicka-data/pocasi/typizace-povetrnostnich-situaci).

3. Analysis of rainfall time structures and precipitation types

3.1. Clustering of 6-h precipitation episodes

The results of clustering of 1950 reference events by half-time concentration indexes values are depicted by a series of parallel graphs in Fig. 3. For $k = 2$, precipitation episodes were divided into rather concentrated (cA_2) and rather steady episodes (cF_2). The frequency of the episodes was similar, with only slightly more episodes in cF_2 (Fig. 4, left column). When increasing the k value, clusters cA_3 and cF_3 became more homogeneous than cA_2 and cF_2, respectively, as a new cluster cE_3 collected episodes of precipitation concentrated into approximately 3 h. The cluster cE_3 obtained its members from both cA_2 and cF_2.

Next clusters cD_4 and cC_5 were characterized by only a small concentration in a longer time window but a much higher concentration in a shorter time window (Fig. 3), which proved a substantial temporary decrease in precipitation intensity or even its interruption during the 6 h. Because the intensity decrease or even the interruption regularly lasted more than 2 h in episodes of cD_4, the cluster originated mainly from cF_3 and cA_3 but not from cE_3. In contrast, the cluster cC_5 was characterized by a short intensity decrease or interruption; therefore, the cluster obtained its members mainly from cA_4 and cE_4, not from cD_4 or cF_4.

When further increasing the k value, subtypes of the already specified variants appeared. Clustering into six clusters enabled episodes lasting approximately 1 h (cB_6) to be distinguished from even shorter ones (cA_6). In fact, this step almost split the cluster cA_5 into halves. Nonetheless, because concentrated precipitation episodes have a crucial role in producing damage, the clustering into six clusters was further considered, unlike division into even more clusters, which would determine subtypes of less concentrated episodes (not presented).

For example, the episode with the absolute maximum R_6 (Fig. 2) was characterized by [C_6; $C_{3,2}$; C_1] values as high as [0.81; 0.30; 0.28] (see Section 2.5). When k was set 2, the episode belonged to the cluster cF_2 because of better correspondence with its typical values [0.39; 0.28; 0.21] than to the typical values of the cluster of concentrated precipitation cA_2 [0.93; 0.70; 0.59]. Nevertheless, it is obvious from Fig. 3 that once the cluster cE_3 was established by increasing the parameter k to 3, the presented episode corresponded much better to this cluster because of its typical values [0.84; 0.39; 0.29]. It was also the case for

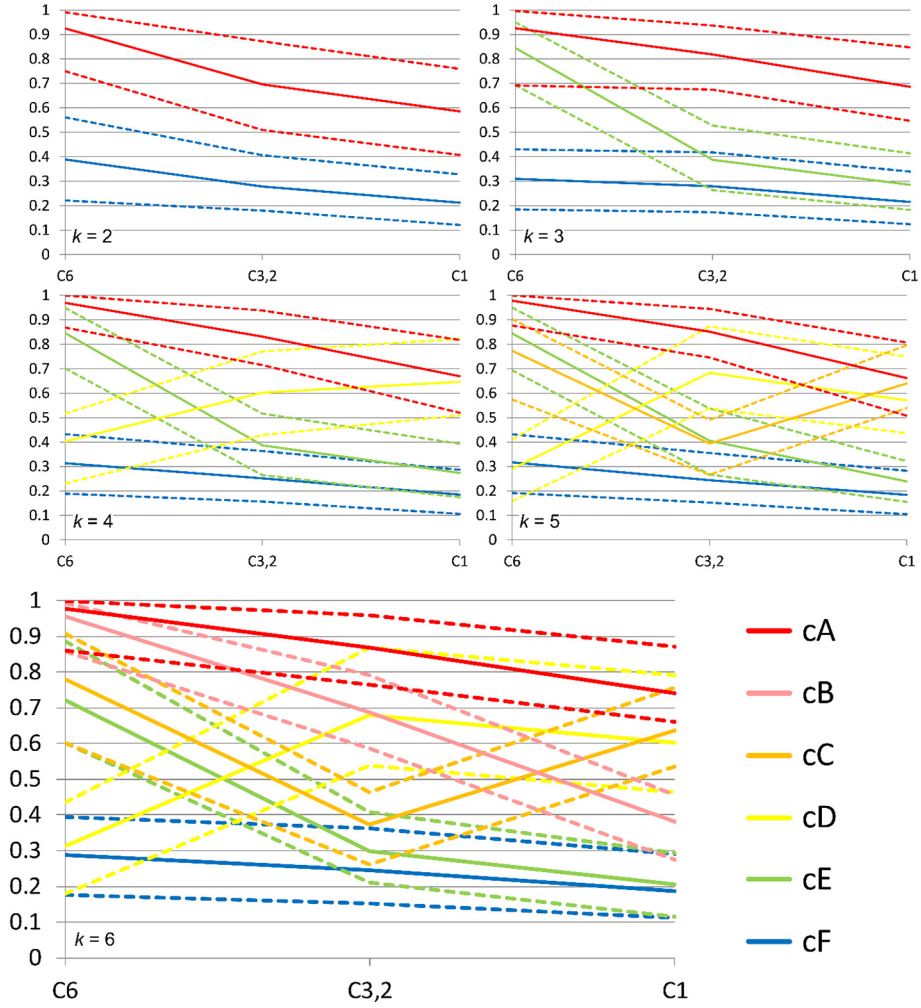

Fig. 3. Parallel coordinate plots of clusters of 6-h precipitation totals resulting from *k*-means clustering for increasing *k*. Each cluster is represented by three lines of the same color in all graphs (if detected) corresponding to quartiles of the parameters used as similarity measures: medians (solid lines) and the 25th as well as the 75th percentiles (dashed lines).

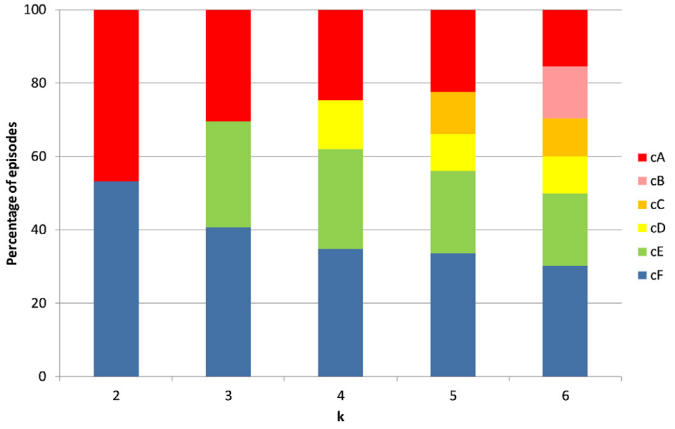

Fig. 4. Percentage of episodes belonging to individual clusters when increasing their number *k*.

each higher *k* value – the episode belonged to cE_4 as well as to cE_5. Finally, *k* equals six and the episode belongs to the cluster cE_6 with its typical values [0.72, 0.30; 0.20] (Fig. 3).

Unlike in Fig. 3, the clusters are represented by all episodes as well as by their centroids in Fig. 5, which demonstrates the variability of episodes within individual clusters as well as relations among them. Neighboring clusters cE_6 and cF_6 only differed with respect to the actual length of precipitation, which was not very concentrated from the viewpoint of short time windows; clusters cC_6 and cD_6 are next to clusters cE_6 and cF_6, respectively; the cluster cB_6 is adjacent to all other clusters apart from cF_6.

3.2. Characteristics of the final clusters

The last column in Fig. 4 confirms that the final clusters were not equally represented by precipitation episodes. The proportion of episodes with steady precipitation intensity (30%, cluster cF_6) was approximately the same as the proportion of the two clusters of most concentrated episodes together (cA_6 and cB_6). The other 20% were uninterrupted episodes lasting approximately 3 h (cE_6), e.g. the absolute maximum R_6 episode from 1 August 2002, see Section 3.1. The last 20% were episodes with substantial temporary decrease of precipitation intensity, or even its interruption (cC_6 and cD_6).

The analysis of episodes from the viewpoint of their magnitude and the ratio between maximum 6-h and 30-min precipitation totals (Fig. 6) proved the crucial role of precipitation concentration in the rainfall time structure variability. Whereas the maximum $R_{0.5}$ always received less than 30% of R_6 in the case of cF_6, it was usually more than 60% in the case of cA_6. Nonetheless, clusters with most concentrated precipitation (cA_6 and cB_6) were not represented among the maximum recorded 6-h episodes. In contrast, not only the absolute maximum R_6

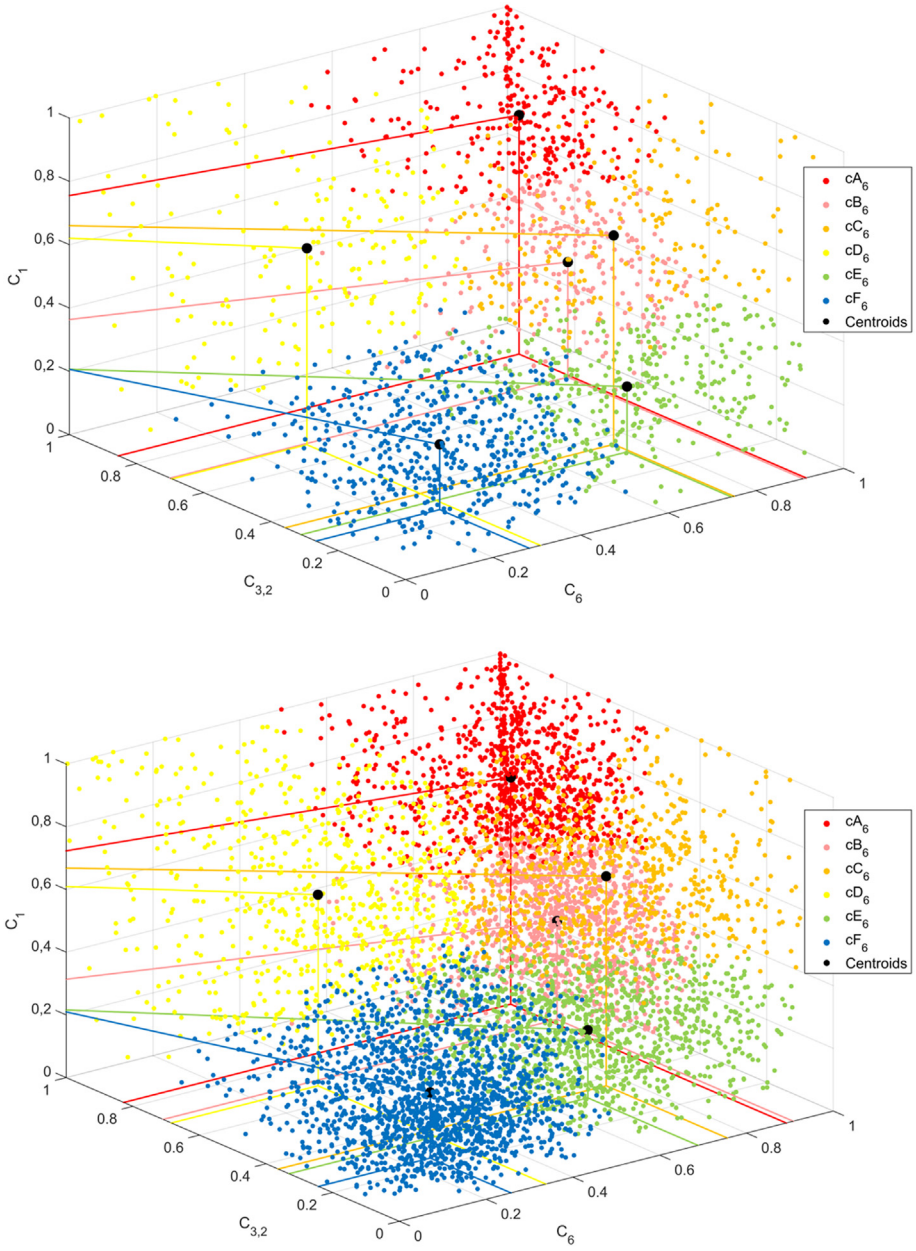

Fig. 5. 3-D scatter plots of the final (above) and control (below) clustering of 6-h precipitation totals, with axes representing values of three parameters used as similarity measures. The clusters are distinguished by colors and represented by their centroids.

episode (Fig. 2) but also other two of four maximum 6-h precipitation totals belonged to cluster cE_6, when maximum $R_{0.5}$ comprised only 25–32% of the maximum R_6. The percentage was generally higher in the case of the composed clusters cC_6 and cD_6, including the second maximum event that belonged to cluster cD_6.

Table 3 compares the absolute maximum R_6 episode from 1 August 2002, belonging to the cluster cE_6, with maximum episodes from other five clusters. Respective hyetographs are presented in Fig. 7. Maximum cA_6 episode was characterized by so high 10-min precipitation intensity maximum (23.1 mm) that the maximum $R_{0.5}$ was almost 60% of the maximum R_6 (Fig. 6) Maximum cB_6 episode lasted only less than two hours but weak precipitation occurred several hours later (Fig. 7); therefore, C_6 did not reach the value 1. After 30 min with maximum precipitation intensity it remained rather high. As the result, the value of C_1 was much lower than in the case of the maximum cA_6 episode. Maximum cC_6 and cD_6 episodes were characterized by the decrease in intensity and even the precipitation interruption, respectively. Though, in case of the maximum cD_6 episode, the interruption was not as long as in most other episodes of the cluster, the episode still belonged there because of continuing precipitation. Finally, the maximum cF_6 episode covered the whole time window with only small increase of precipitation intensity in its second half. In fact, the episode was only a part of a much longer event lasting several days and producing catastrophic flooding mainly in Poland (Kašpar et al., 2013).

3.3. Construction of synthetic storm hyetographs

When expressed as the cumulative percentage of 6-h rainfall, hyetographs of selected precipitation episodes (Fig. 8) demonstrated common features of the clustered precipitation episodes and proved that the clustering significantly reduced the variability of episodes in comparison with the entire dataset (compare with Fig. 1). However, the half-time concentration indexes did not specify when the maximum occurred within the 6-h time window and how the precipitation

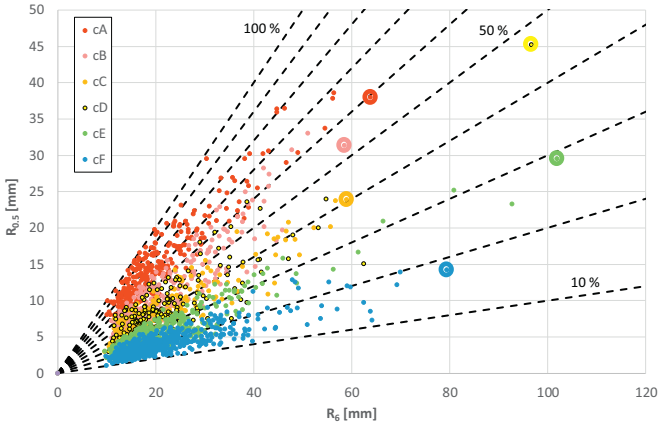

Fig. 6. Maximum 30-min rainfall $R_{0.5}$ within the considered 6-h precipitation totals R_6. The clusters are distinguished by colors according to the legend. Dashed lines represent the ratio $R_{0.5}/R_6$ from 10 to 100%. Maximum episodes from each cluster are highlighted (compare with Table 3).

intensity was distributed during the rest of the episode. Differences in precipitation intensity timing produced smoothing of the mean curves and thus prevented us from simply using means as synthetic storm hyetographs for the clusters. This smoothing was mainly pronounced in more concentrated clusters such as A_6 or B_6.

Therefore, the suggested construction method was based on averaging relative precipitation intensities (compared with R_6) in the following way. Instead of averaging the precipitation intensities in corresponding time windows, the episodes were first divided into sections with respect to their precipitation intensity (see examples for each cluster in Fig. 7). We searched for the main section in individual episodes, defined as 30 min with the maximum $R_{0.5}$. Next, we searched for such a 1-h section with maximum R_1 in which the main section was fully nested. The 1-h section thus consisted of the main section and one or two side sections. Analogously, we searched for 2-h and 3-h sections with maximum R_2 and R_3, respectively, which enabled the determination of the next side sections. Therefore, each precipitation episode from clusters cA_6, cB_6, cE_6, and cF_6 was divided into one main section (lasting 30 min) and several side sections (lasting altogether 330 min) that could both precede and/or follow the main section. The sections were characterized by percentages of R_6 and by their length.

For clusters cC_6, and cD_6, characterized by a substantial temporary decrease of precipitation intensity or even its interruption, we determined two independent main sections lasting 30 min each within each precipitation episode. The side sections were determined only by the maximum 1-h section in the case of cluster cC_6 and by maximum 1-h and 2-h sections in the case of cluster cD_6. If side sections belonging to the two main sections still overlapped, the side section belonging to the weaker main section was shortened. Each precipitation episode from clusters cD_6 and cC_6 was thus divided into two main sections (2×30 min) with up to two (cC_6) or four (cD_6) side sections between them and possibly several other side sections that preceded the first main section and/or followed the second main section.

The characteristics of the main and side sections were averaged across all episodes of the given cluster. The procedure began by averaging the main sections. Because they had the unified duration of 30 min, we determined their mean timing as well as the mean relative precipitation intensities during the three 10-min windows that composed the main sections. The sequence of mean side sections was then determined, starting with the side sections comprising the maximum 1-h totals together with the main section. Side sections both before and after the main sections were characterized by their average length and the mean relative precipitation intensities in the 10-min step. The averaged sections were then connected into curves with a time resolution of 1 min and eventually smoothed by a 10-min moving average to remove sudden precipitation intensity changes at the edges of the considered sections (Fig. 9). However, this procedure would underestimate the mean maximum 1-min precipitation intensity because it would only equal the mean maximum 10-min precipitation intensity. Therefore, the increase of the mean intensity from the previous 10-min window as well as the decrease of the mean intensity into the next 10-min window were linearly extrapolated into the maximum 10-min window. The maximum 1-min precipitation intensity was determined as the intersection point of the two lines.

Fig. 9 presents the final synthetic storm hyetographs for the six clusters. We call them camel hyetographs because of their characteristic shapes with one or two peaks. Cluster cA_6 is characterized by the maximum temporal concentration of precipitation. On average, 72% and 85% of the 6-h precipitation total fell during 30 and 60 min, respectively, with maximum 1-min precipitation intensity greater than 3.7% of R_6. Another typical feature is the significantly faster increase of the intensity than its subsequent decrease, which remained true in the case of cB_6, when almost 50% and 73% of R_6 appeared during 30 and 60 min, respectively. Clusters cC_6 and cD_6 are characterized by the mean distance between two maxima of precipitation intensity lasting 102 and 228 min, respectively. In both cases, the first maximum was usually higher than the later one. On average, the first 1-min intensity maximum was 148% and 142% of the second maximum in cC_6 and cD_6, respectively. The first maximum was also more pronounced in terms of the percentage of precipitation during the main 30-min sections (the percentages were 34% and 25% for cC_6 and 33% and 24% for cD_6). In cluster cE_6, precipitation was even less concentrated, with maxima of 27% and 45% during 30 and 60 min. Finally, episodes from the cluster of rather steady precipitation intensity (cF_6) were also usually not fully uniform from the viewpoint of precipitation course, with maxima of 19% and 31% during 30 and 60 min. (If precipitation intensity was absolutely steady during an episode, the maxima during 30 and 60 min would be 8% and 17%, respectively). The presented characteristics of the clusters are valid for the studied region, although some of them could probably be more widely applicable.

3.4. Precipitation types associated with the clusters

The six clusters of reference events significantly differ in terms of the type of precipitation episodes comprising them (Fig. 10a). Convective and mixed episodes dominated in cluster cA_6 characterized by the steepest hyetograph (71.5 and 24%, respectively). Also in the

Table 3
Characteristics of maximum 6-h precipitation (R_6) episodes of six determined clusters. The episodes are characterized by three half-time concentration indexes C_6, $C_{3,2}$, and C_1 (see Section 2.5) as well as by the ratio $R_{0.5}/R_6$ (see Section 3.2). The location of the radar pixels where the episodes were detected is presented in Fig. 1.

Cluster	Start of the episode [dd/mm/yyyy hh:mm]	Location	R_6 [mm]	C_6	$C_{3,2}$	C_1	$R_{0.5}/R_6$
cA_6	23/07/2010 18:10	Kuchařovice	63.9	0.96	0.64	0.64	0.59
cB_6	19/08/2007 19:20	Praha	58.5	0.90	0.80	0.36	0.54
cC_6	23/07/2010 19:00	Brno	59.0	0.79	0.48	0.53	0.40
cD_6	21/06/2006 21:30	Pardubice	96.7	0.63	0.67	0.66	0.47
cE_6	01/08/2002 18:10	Luká	101.9	0.81	0.30	0.28	0.29
cF_6	16/05/2010 20:40	Lysá hora	79.4	0.39	0.25	0.09	0.18

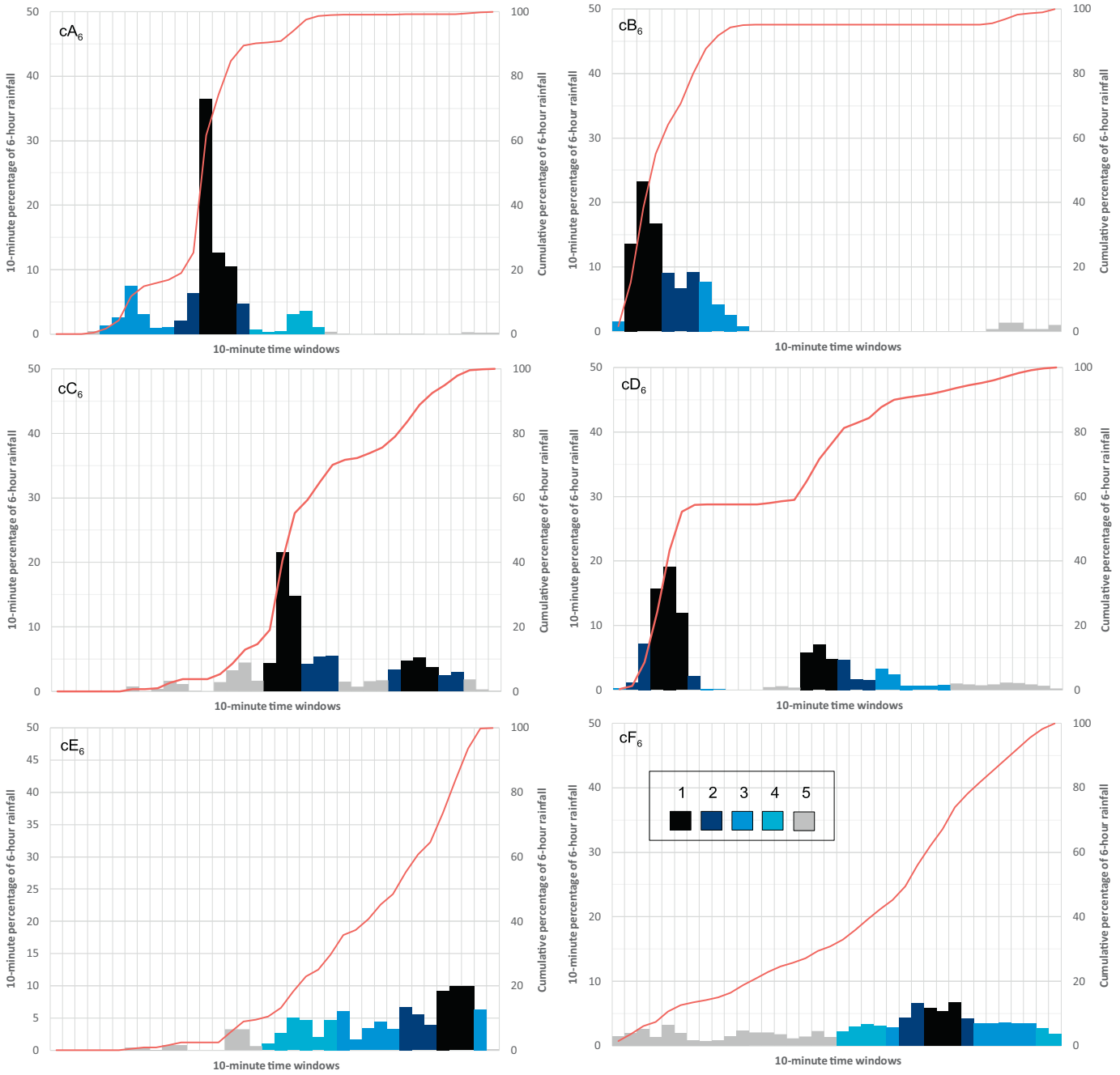

Fig. 7. Hyetographs of episodes with absolute 6-h precipitation maximums for 6 distinguished clusters detected in one of 39 radar pixels corresponding to Czech synoptic weather stations; the episodes are further characterized in Table 3. The sections of the episodes are distinguished with respect to the legend: 1 – the main section(s); 2, 3, 4, and 5 – the side section(s) completing the maximum R_1, R_2, R_3, and R_6, respectively.

similar cluster cB_6, stratiform episodes were rather rare (10%). On the contrary, the cluster of long-lasting episodes (cF_6) was almost completely comprised of stratiform (78%) or mixed (19%) precipitation. Episodes with steady intensity lasting about three hours (cE_6) were also mainly stratiform (45%) or mixed (36%) while two variants represented by "two-humped" hyetographs (cC_6 and cD_6) were more frequently mixed (44.5% and 37%) or convective (41 and 38.5%).

If concerning the precipitation types, only 6% of 459 detected stratiform episodes belonged to clusters cA_6 or cB_6 (Fig. 10b) Other less than 4% stratiform episodes lasted about three hours but with a significant precipitation intensity decrease meanwhile (cluster cC_6). It confirms the fact that purely stratiform episodes are usually characterized by rather steady precipitation intensity for about three hours at least (cluster cE_6, 23%) but even more frequently they last longer (cluster cF_6 or possibly cD_6, altogether more than 67% of stratiform episodes). For example, the maximum episode of the cluster cF_6 (see Table 3) was fully stratiform. The weather state was reported by the code 69 (moderate to heavy rain and snow) for all six hours which corresponds with the steady precipitation intensity in Fig. 7.

On the contrary, if a long-lasting episode was purely convective, its intensity usually fluctuated. Thus, only 3% of convective episodes belonged to the cluster cF_6 (Fig. 10d). Instead, such long convective episodes belonged four times more frequently to the cluster cD_6 because of a precipitation intensity decrease or even an interruption usually occurred meanwhile. This also happened during the maximum cD_6 episode (Table 3). It was fully convective with six weather state

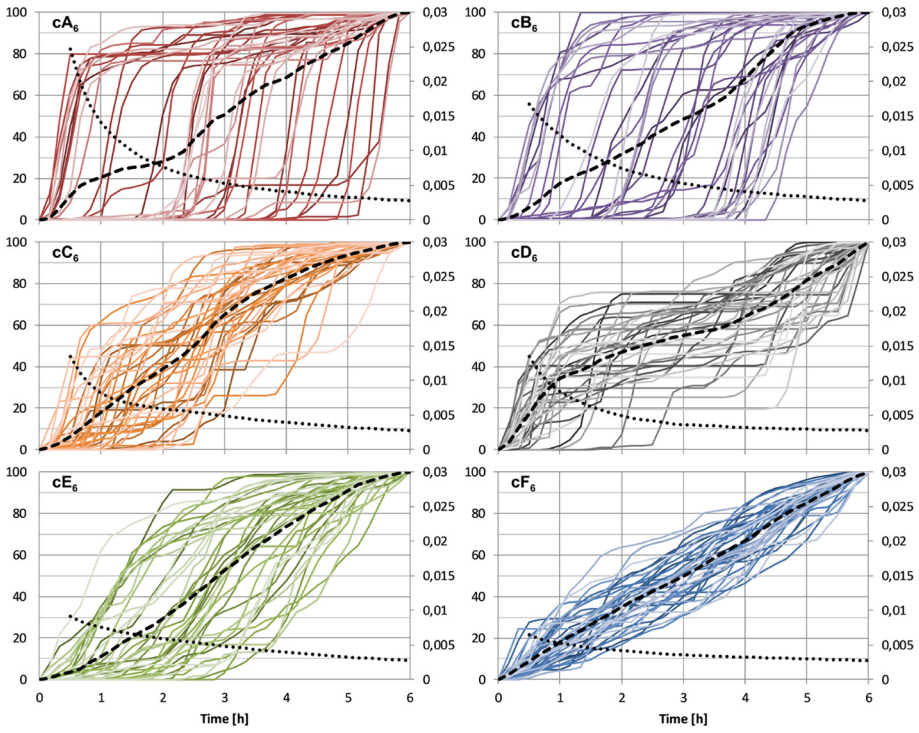

Fig. 8. Normalized hyetographs of 6-h precipitation maxima for 6 distinguished clusters in 39 radar pixels corresponding to Czech synoptic stations, expressed as cumulative percentage of 6-h rainfall (left axis, in %). The color shades represent the magnitude of the totals from the highest value (dark) to the lowest value (light). Dashed lines depict the means of the 39 hyetographs in each graph. Dotted lines indicate the typical maximum average intensity curves standardized by 6-h totals (right axis, in min^{-1}). The curves follow the average values in each cluster between 30 min (length of main sections, see Section 3.3) and 360 min (episode duration) with the time step of 10 min (temporal resolution of input data).

observations as follows: 97, 97 (heavy thunderstorm), 80 (light rain showers), 95, 95 (light to moderate thunderstorm), and 91 (thunderstorm in past hour, currently only light rain). The observations corresponded very well with the hyetograph (Fig. 7), characterized by the interruption of heavy rains during the third hour of the episode.

Other 25% of purely convective episodes lasted about three hours with or without a remarkable precipitation intensity decrease and belonged to clusters cC_6 or cE_6, respectively (Fig. 10d). For example, the absolute maximum R_6 episode from 1 August 2002 was of this character (see Section 2.6). Nevertheless, the majority of purely convective episodes (more than 61%) belonged to the clusters cA_6 and cB_6 characterized by only one precipitation intensity maximum lasting about 30 min or one hour, respectively. Because the cA_6 maximum (Table 3) was not covered with manual observations at the respective weather station, the precipitation type could not be recognized. Nevertheless, the next maximum R_6 value in the cluster cA_6 (56.2 mm on 17 July 2010 in the grid point which station Přibyslav is in) was fully convective because of the weather state 95 (light to moderate thunderstorm) reported throughout the episode.

The mixed precipitation episodes were rather equally distributed among the six clusters (Fig. 10c). The reason is that the clusters cC_6 and cD_6, where the percentage of mixed representation episode was maximum, are less frequent than the others (compare Figs. 8a and 4). If convective and stratiform parts of an episode followed one after another, the convective one was the first one much more frequently, mainly in clusters cA_6, cB_6, cC_6, and cD_6. In the other two clusters, convective and stratiform parts are more randomly distributed within the episodes which may be due to convective phenomena nested into larger stratiform precipitation.

Both the cB_6 and cC_6 maximum episodes (Table 3) were reported as mixed at given weather stations but the weather state related to stratiform precipitation appeared only at the end of the episode in both cases. It can be deduced from the shapes of their hydrographs (Fig. 7) that in fact, the cB_6 maximum was almost purely convective because only the negligible precipitation at the end of the time window was stratiform. On the contrary, the cC_6 maximum was a really mixed episode because the second main section of the event was stratiform.

3.5. Circulation patterns related to the clusters

According to the CHMI classification, six of 28 defined types seem to be most typical for 6-h precipitation episodes in Czechia: Bp – moving through (23%); C – cyclone above Central Europe (15%); SWc_2 – one of three south-western cyclonic types (9% or even 17.5% if considered together with other two SWc types); NEc – northeastern cyclonic type (9%); B – stationary through (9%); Ec – eastern cyclonic type (8%). The percentage of all six types among precipitation episodes (altogether 73%) was substantially higher than their percentage among all days of the study period (altogether 39%), see Fig. 11. Moreover, significant differences among the presented clusters were detected with respect to the relation between the frequency of the types and episodes.

The clusters with rather concentrated precipitation episodes (cA_6, cB_6, cC_6) are very similar with respect to circulation patterns producing them. In all clusters, the types Bp, SWc_2, Ec, and B were responsible for 58–59% of episodes. While the percentage of both circulation types characterized by a trough (Bp, B) was similar among the three clusters and among all precipitation episodes, the frequency of other two types (SWc_2, Ec) was enhanced by almost 50% in the clusters cA_6, cB_6, and cC_6. It was probably due to the fact that both the south-western and eastern cyclonic types are favorable for convective rains which dominated mainly in clusters cA_6 and cB_6 (Fig. 10a).

Nevertheless, the maximum episodes of clusters cA_6, cB_6, and cC_6 were connected with troughs. Both the cA_6 and cC_6 maximum appeared on 23 July 2010 (Table 3) when the circulation pattern was classified as Bp. A significant slowly moving cold front divided warm and moist air above eastern Europe from much colder air to the west. Along the trough, severe convective storms moved to the north. Nevertheless, the type of precipitation was classified as mixed in Brno-Tuřany because of the following stratiform rain. Though the cB_6 maximum on 19 August 2007 was also classified as mixed, it was almost completely convective (see Section 3.4). The synoptic pattern was dominated by a stationary trough (type B).

The dominance of the most frequent type Bp was even higher within clusters cD_6 and cE_6 (Fig. 11). While the types Bp and B were responsible for all three types of precipitation in these clusters, the other four types were more specialized. The type C (central cyclone)

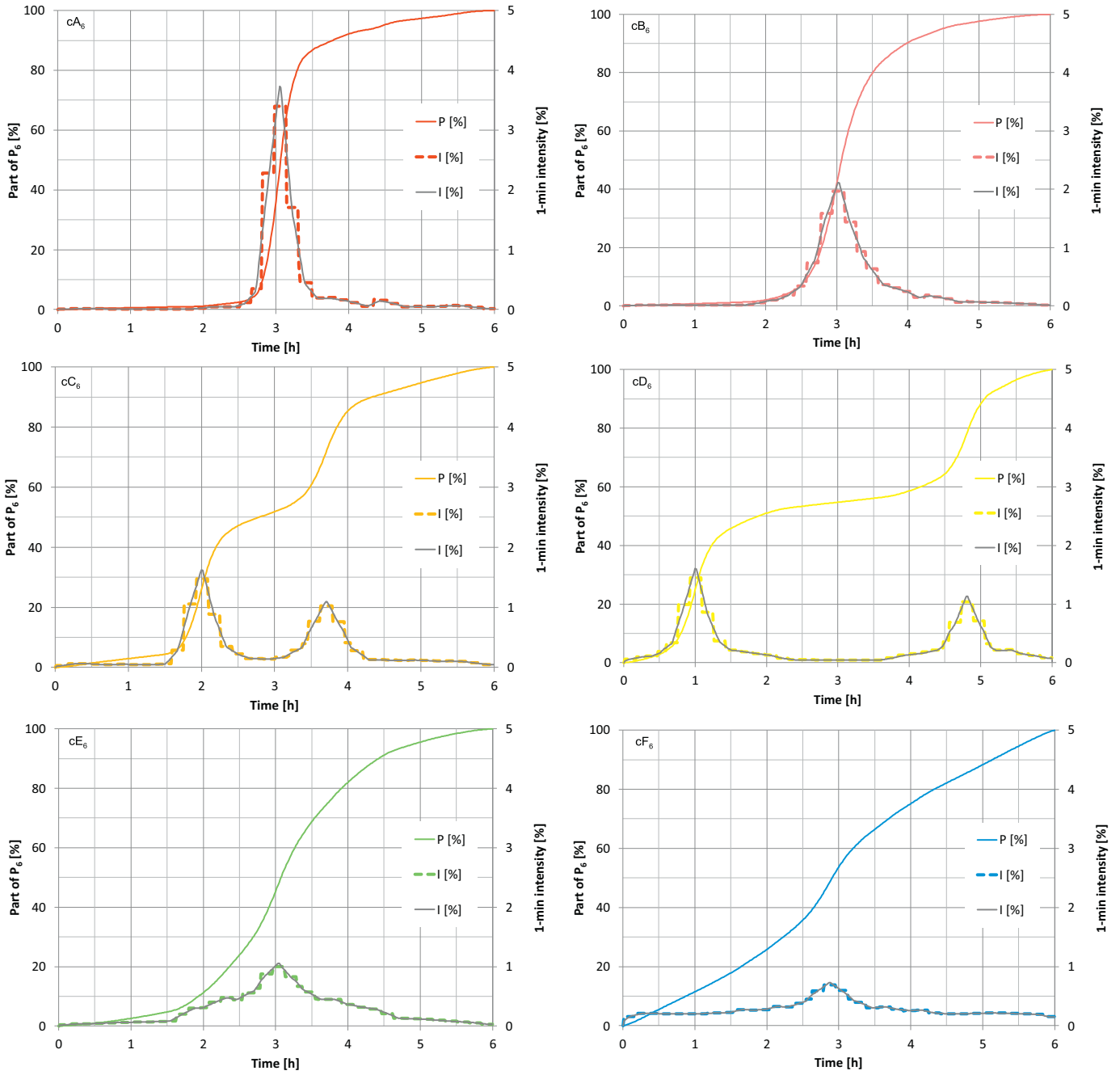

Fig. 9. Synthetic storm hyetographs for 6 distinguished clusters. Dashed lines indicate the hyetographs before smoothing by the moving average and enhancement of the maximum 1-min precipitation intensity.

produced 16% and 25% of stratiform but only 4% and 2% of convective episodes in clusters cD_6 and cE_6, respectively. The effects of the type NEc were similar: 19% and 16% of stratiform but only 8% and even 0% of convective episodes in clusters cD_6 and cE_6, respectively. On the contrary, the type Ec was associated with convective episodes rather than with stratiform ones, mainly in the cluster cE_6. Regarding the type SWc_2, it produced even no stratiform episode but 10% and 14% of convective and mixed episodes in the cluster cD_6, respectively.

The maximum episodes of clusters cD_6 and cE_6 (Table 3), both due to convective rains, were associated with circulation patterns favorable to them. The maximum cD_6 episode appeared during a south-western cyclonic situation in extra warm, moist and unstable air (dew point 20.6 °C in Pardubice at 18 UTC; CAPE as high as 1379 J/kg on 22 July at 00 UTC at the aerological station Prostějov). The maximum cE_6 episode with the highest recorded R_6 was associated with the type Ec. Easterly from an upper-level cut-off low above France, central Europe was covered by very moist air (dew point 18.9 °C in Luká at 11 UTC). Rather favorable convective environment was confirmed by many indexes calculated from the Prague sounding at 12 UTC, e.g., K-index 30.2; (http://www.weather.uwyo.edu/upperair/).

The cluster cF_6 with long-lasting, mainly stratiform rains (Fig. 10a) was the only one which the type Bp did not dominate in. Two synoptic patterns favorable to stratiform rains, namely C and NEc, produced 30% and 16% of the episodes, respectively. The type NEc was responsible also for the maximum episode of the cluster which was fully stratiform and was detected on 16/17 May 2010 in Moravsko-Slezské Beskydy Mts. (see Table 3). The whole precipitation event lasted more than three days as it was connected with a Vb cyclone with the center remaining

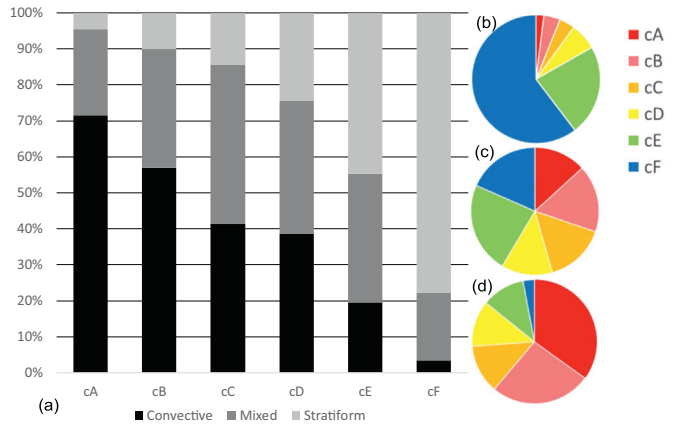

Fig. 10. Percentage of convective/mixed/stratiform precipitation episodes belonging to individual clusters (a) and percentage of the clusters among the set of stratiform (b), mixed (c), and convective episodes (d).

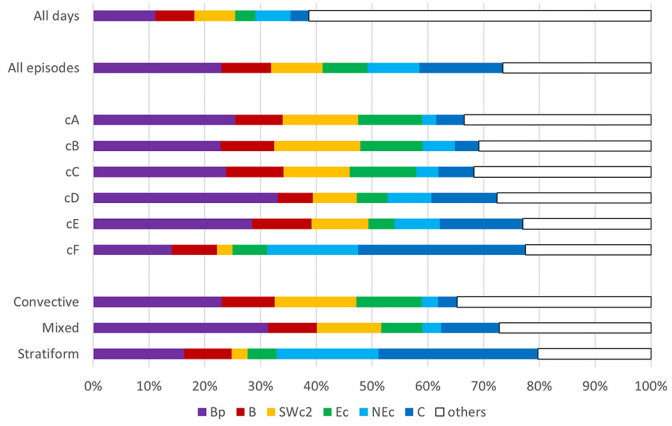

Fig. 11. Percentage of synoptic patterns among all days from May to September, among all classified episodes, among six clusters of them, and among the episodes of three types with respect to the precipitation type.

for unusually long time above south-west Ukraine. As the result, heavy rains occurred and were further orographically enhanced in the mountains due to the strong northerly winds (Kašpar et al., 2013).

4. Discussion of the results

The suggested procedure was tested regarding several aspects that could influence the results. First, a control clustering was run with a different definition of reference precipitation episodes (Section 4.1). In Section 4.2, we discuss how the selected length of the time window could affect the results. Finally, Section 4.3 compares our methodology with other approaches.

4.1. Robustness of the clustering

The determination of clusters representing variants of rainfall time structure in Czechia was repeatedly performed to optimize the suggested procedure. After these experiments, the number of employed half-time concentration indexes was set to three because the result clusters were less consistent in cases of higher numbers of the indexes. The combined index $C_{3,2}$ was introduced because if only one of its parts ($R_{1.5}/R_3$ or R_1/R_2) was used, a time gap would occur among the indexes.

To demonstrate the robustness of the final product, we present a comparison with a control run of clustering with a dataset that differed from the original one (Section 2.4) in the numbers of both the

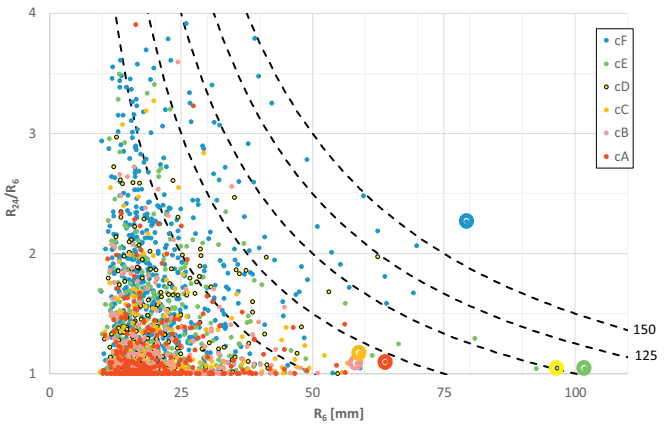

Fig. 12. Ratio between maximum 24-h and 6-h precipitation totals (R_{24}/R_6) as a function of R_6 for the reference 6-h episodes. The clusters are distinguished by colors according to the legend. Dashed lines represent isolines of R_{24}. Maximum episodes from each cluster are highlighted (compare with Table 3).

considered pixels and maximum episodes. Instead of 50 maxima from 39 pixels representing the locations of Czech synoptic weather stations, only 10 maxima were used in the control run, although they were from 651 pixels representing locations of all rain gauges used in the adjustment of radar data (Section 2.3).

The results of the control run of clustering depicted in Fig. 5 can be easily compared with the original clustering presented in the paper. The comparison proves that the final product remains almost the same regardless of the number of employed episodes, as well as the location of pixels in which the episodes were detected.

4.2. Effects of the time window length

Because daily totals are frequently used for analysis of rainfall time structures, the relationship among the 6-h and the 24-h totals was presented in Fig. 12. It demonstrates that the three maximum reference episodes did not substantially exceed the 6-h time window. As was expected, 6-h episodes with steady precipitation intensity (cF_6) only rarely remained without additional precipitation. Frequently, the maximum R_{24} was more than twice as high as R_6 in this cluster. In contrast, most concentrated episodes from the cluster cA_6 were much less frequently accompanied by other significant precipitation outside the 6-h time window; if it occurred, it was often because of the diurnal cycle of convective rains when another intense precipitation episode was repeated at the same place after more than 18 h (not depicted). The difference between the clusters cA_6 and cF_6 is even more pronounced if only major episodes are considered (e.g., with R_6 above 40 mm).

A simultaneous examination of Figs. 6 and 12 enables comparison of how the clusters were represented among the maximum values of $R_{0.5}$, R_6, and R_{24} of the reference episodes. The 30-min totals above 30 mm all belonged to clusters cA_6 or cB_6., with only the one exception of an extra strong episode from cluster cD_6. In contrast, the 6-h totals above 60 mm were mainly because of episodes from clusters cE_6 or cF_6. Finally, the last-mentioned cluster of rather steady rainfall significantly dominated the 24-h maxima. Future research should confirm substantial regional differences that mainly arise because of orography.

4.3. Comparison between half-time concentration indexes and other approaches

The current representative of the most related approaches is the so-called n-index by Monjo (2016), a very promising concept reporting on the temporal variability of rainfall behavior during a precipitation episode. The n-index is inspired by the observed rainfall self-similarity at several time scales and actually acts as a fractal dimension of the

maximum average intensity (hereinafter MAI) over given periods. The index is defined as the exponent of the power law relating the MAI and the length of an averaging time interval, and postulates the decrease of the MAI provided that the length of the interval is increasing:

$$I(t) = I(t_0)\left(\frac{t_0}{t}\right)^n \tag{9}$$

where $I(t)$ and $I(t_0)$ are the MAI corresponding to lengths of the time interval t and t_0, and n is the n-index, a dimensionless parameter reaching values from 0 to 1.

The unquestionable advantage of the n-index is that it is generally independent of the intensity and episode duration. As other methods, the n-index is sensitive to the temporal resolution of input data (Monjo, 2016); specifically, it may lead, in our opinion, to unrealistic high MAIs for $n \rightarrow 1$ and $t << t_0$. Nevertheless, it is still an ideal tool with wide application for the extrapolation/interpolation of the behavior of the rain rate for several time intervals. We realized that its primary purpose was not the construction of synthetic storm hyetographs, so we tried to find an alternative approach. Although, the employment of episodes of fixed duration is in contradiction with one of advantages of the n-index, we present a brief comparison between the approaches in the following text.

Fig. 13 shows a good link of the n-index with clusters of episodes that are characterized by synthetic storm hyetographs consisting of one intensity maximum. The high bipolarity of the clusters cA and cF reflects on the highest difference between corresponding n-indexes and thus also between shapes of corresponding MAI curves (Fig. 9). The average value of the n-index is 0.86 for the cluster cA and 0.33 for the cluster cF. According to Monjo (2016), this classifies the cluster cA and cF into irregular and regular rainfall regime, respectively, which is in accordance with our findings (see Section 3.3).

Some episodes, however, which are equivalent in terms of the n-index, may not be equivalent in view of the hydrological response to them for a given precipitation total. In particular, this is noticeable for the clusters cD and cC that are characterized by hyetographs with more complex shape (Kottegoda et al., 2014). The cluster cD, the hyetograph of which consists of two relatively short periods of increased intensity separated by a break in rainfall, is linked to similar n-index values (Fig. 13) as the cluster cB, which is related to significantly higher time concentration of precipitation in 6-h period. Moreover, the cluster cC is unexpectedly closer in this sense to the cluster cE than the cluster cD, which is related to less time concentration of precipitation. Aiming at the applicability in hydrological modelling is one of main reasons we quantified the intensity decrease with increasing length of the time interval in a way similar to Monjo (2016) but using three indexes that are both independent and self-consistent (see Section 2.5). A seeming disadvantage of our approach may be the use of the fixed 6-h time window when detecting episodes. Nevertheless, the methodology applied is in principle transferable to episodes of various duration, though we found 6-h totals to be suitable for our purposes and requirements (see Section 2.4).

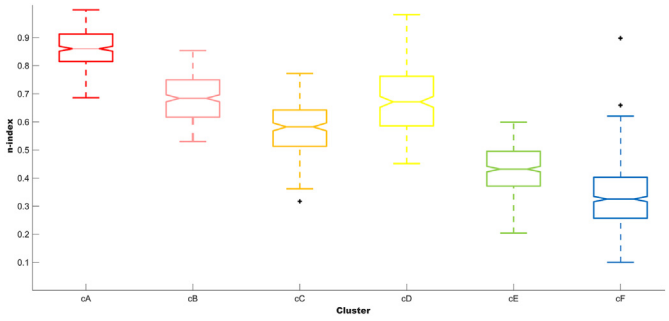

Fig. 13. Distribution of values of the n-index for 6 distinguished clusters of episodes; n-index values were estimated according to Monjo (2016) using the reference time t_0 = 10 min and values of t between 30 and 360 min with the time step of 10 min (see Eq. (9)). Each box plot depicts the median, 25th and 75th percentiles, and potential outliers (values that are more than 1.5 times the interquartile range away from the 75th or 25th percentile).

5. Conclusions

We believe that synthetic storm hyetographs should be constructed in several variants in regions with large variability of rainfall time structures, as in Czechia. Although a local study could be based on rain gauge data alone, future regional applications require radar-based data series with high temporal resolution and adjusted by rain gauge data. The 6-h totals were selected as a basic value for characterizing a precipitation episode because on one hand, the local effect of a rainstorm is mainly influenced by the short-term precipitation intensity; on the other hand, 6 h are long enough to enable the analysis of the precipitation time structure. Sensitivity analysis confirmed the relationship between the precipitation intensity course during 6 h and even for 24-h precipitation totals.

The study period lasted 10 years and included numerous heavy rains of mainly stratiform and convective characters as in August 2002 (Řezáčová et al., 2005) and August 2010 (Sokol et al., 2014), respectively. As reference episodes, 1950 maximum 6-h totals were selected within 39 radar pixels in which Czech synoptic weather stations are located (50 episodes per pixel, which means one episode per month on average). Sensitivity analysis confirmed that the results did not significantly depend on the number of considered episodes.

Reference episodes were clustered by the k-means method with respect to three half-time concentration indexes. The study confirmed that the suggested indexes enabled variants of episodes to be distinguished with respect to the time distribution of precipitation intensity. From a sequence of clustering with step-by-step increasing numbers of clusters k, the selected product comprised six clusters that represented all main shapes of the hyetographs. One determined cluster represented steady precipitation intensity during the entire episode, three others distinguished variants of more concentrated episodes and the two remaining clusters collected 20% of the episodes characterized by a substantial temporary decrease of precipitation intensity or even its interruption during the episode.

Because of differences in the timing of maximum precipitation intensity during the maximum 6-h episodes, the synthetic storm hyetographs could not be constructed by the simple averaging of 10-min totals. To preserve the main features of the episodes, they were disaggregated with respect to the precipitation intensity into main 30-min sections and adjacent side sections. Synthetic storm hyetographs were then compiled from these sections averaged across all episodes of the given cluster; we called them camel hyetographs because of their characteristic shapes with one or two peaks. Four “one-humped” hyetographs differed from each other in the magnitude of the peak; the main difference between the two remaining “two-humped” hyetographs was the different distance between their peaks.

Determined six clusters of precipitation episodes were analyzed from the viewpoints of precipitation types producing them. Substantial differences among the clusters were detected. In general, the percentage of stratiform or convective precipitation increased with the increasing or decreasing length of the episodes, respectively. The results correspond with differences in synoptic patterns producing the episodes in various clusters. The link between the meteorological causes and the rainfall time structures enables our future research which will consider frequency analysis of the determined six clusters of precipitation episodes throughout the entire study area. Initial results indicate that the percentage of the clusters significantly differs with respect to the topography, the length of precipitation events, and even the extremity of precipitation totals. Combination of return levels of the synthetic storm hyetographs opens the door to an improvement of the design of the storm hyetographs and the local hydrological response of the episodes

at the local scale. Finally, the research will be expanded to consider the spatial structure of precipitation episodes.

Acknowledgments

This work was supported by the Czech Science Foundation [grant number 17-23773S] and the Czech Ministry of Agriculture [grant number QJ1520265]. Acknowledgements belong to the Czech Hydrometeorological Institute for radar and rain gauge data and to Zbyněk Sokol, who provided us with the adjustment procedure.

References

Alfieri, L., Laio, F., Claps, P., 2008. A simulation experiment for optimal design hyetograph selection. Hydrol. Process. 22, 813–820.
Amengual, A., Homar, V., Jaume, O., 2015. Potential of a probabilistic hydrometeorological forecasting approach for the 28 September 2012 extreme flash flood in Murcia, Spain. Atmos. Res. 166, 10–23.
Arthur, D., Vassilvitskii, S., 2007. K-means+ +: the advantages of careful seeding. In: SODA '07: Proceedings of the Eighteenth Annual ACM-SIAM Symposium on Discrete Algorithms, pp. 1027–1035.
Bližňák, V., Kašpar, M., Müller, M., 2018. Radar-based summer precipitation climatology of the Czech Republic. Int. J. Climatol. 38, 677–691.
Brádka, J., Dřevikovský, A., Gregor, Z., Kolesár, J., 1961. Počasí na území Čech a Moravy v typických povětrnostních situacích. HMÚ, Prague (in Czech).
Dai, Q., Han, D., Zhuob, L., Huang, J., Islame, T., Srivastava, P.K., 2015. Impact of complexity of radar rainfall uncertainty model on flow simulation. Atmos. Res. 161–162, 93–101.
Desbordes, M., 1978. Urban runoff and design storm modelling. In: Proceedings in International Conference on Urban Storm Drainage, Southhampton.
Ellouze, M., Abida, H., Safi, R., 2009. A triangular model for the generation of synthetic hyetographs. Hydrol. Sci. J.-J. Sci. Hydrol. 54, 287–299.
Guan, M., Sillanpää, N., Koivusalo, H., 2015. Storm runoff response to rainfall pattern, magnitude and urbanization in a developing urban catchment. Hydrol. Process. 30, 543–557.
Hailegeorgis, T.T., Alfredsen, K., 2017. Analyses of extreme precipitation and runoff events including uncertainties and reliability in design and management of urban water infrastructure. J. Hydrol. 544, 290–305.
Urban hydrology, 1986. Urban Hydrology for Small Watersheds. Technical Report. US Department of Agriculture, Washington, pp. 55.
Kašpar, M., Müller, M., 2008. Selection of historic heavy large-scale rainfall events in the Czech Republic. Nat. Hazards Earth Syst. Sci. 8, 1359–1367.
Kašpar, M., Müller, M., Pecho, J., 2013. Comparison of meteorological conditions during May and August 2010 floods in Central Europe. AUC Geogr. 48, 27–34.
Kaufman, L., Rousseeuw, P.J., 1990. In Finding Groups in Data: An Introduction to Cluster Analysis. John Wiley & Sons, Hoboken.
Keifer, C.J., Chu, H.H., 1957. Synthetic storm pattern for drainage design. ASCE J. Hydraul. Div. 83 (HY4), 1–25.
Kottegoda, N.T., Natale, L., Raiteri, E., 2014. Monte Carlo Simulation of rainfall hyetographs for analysis and design. J. Hydrol. 519, 1–11.
Kulasová, B., Šercl, P., Boháč, M., 2004. Verifikace metod odvození hydrologických podkladů pro posuzování bezpečnosti vodních děl za povodní. Technical report (in Czech). Praha, Czech Hydrometeorological Institute (127 pp).
Kunkel, K.E., Easterling, D.R., Kristovich, D.A.R., Gleason, B., Stoecker, L., Smith, R., 2012. Meteorological causes of the secular variations in observed extreme precipitation events for the conterminous United States. J. Hydrometeorol. 13, 1131–1141.
Leon, D., French, J.R., Lasher-Trapp, S., Blyth, A.M., Abel, S.J., Ballard, S., Barrett, A., Bennett, L.J., Bower, K., Brooks, B., Brown, P., Charlton-Perez, C., Choularton, T., Clark, P., Collier, C., Crosier, J., Cui, Z., Dey, S., Dufton, D., Eagle, C., Flynn, M.J., Gallagher, M., Halliwell, C., Hanley, K., Hawkness-Smith, L., Huang, Y., Kelly, G., Kitchen, M., Korolev, A., Lean, H., Liu, Z., Marsham, J., Moser, D., Nichol, J., Norton, E.G., Plummer, D., Price, J., Ricketts, H., Roberts, N., Rosenberg, P.D., Simonin, D., Taylor, J.W., Warren, R., Williams, P.I., Young, G., 2016. The COnvective Precipitation Experiment (COPE): investigating the origins of heavy precipitation in the southwestern UK. B. Am. Meteorol. Soc. 97, 1003–1020.
Libertino, A., Allamano, P., Claps, P., Cremonini, R., Laio, F., 2015. Radar estimation of intense rainfall rates through adaptive calibration of the Z-R relation. Atmosphere 6, 1559–1577.
Manzato, A., Cicogna, A., Pucillo, A., 2016. 6-hour maximum rain in Friuli Venezia Giulia: climatology and ECMWF-based forecasts. Atmos. Res. 169, 465–484.
Michelson, D., Einfalt, T., Holleman, I., Gjertsen, U., Friedrich, K., Haase, G., Lindskog, M., Jurczyk, A., 2005. Weather radar data quality in Europe - quality control and characterization. Working document, COST Action 717, Luxembourg.
Monjo, R., 2016. The n-index and rainfall time structure. Clim. Res. 67, 71–86.
Müller, M., Kašpar, M., Valeriánová, A., Crhová, L., Holtanová, E., Gvoždíková, B., 2015. Novel indices for the comparison of precipitation extremes and floods: an example from the Czech territory. Hydrol. Earth Syst. Sci. 19, 4641–4652.
Novák, P., 2004. Czech weather radar data utilization for precipitation nowcasting. In: Proceedings of ERAD, pp. 459–463.
Novák, P., Kráčmar, J., 2002. New data processing in the Czech weather radar network. In: ERAD Publication Series. 1. pp. 328–330.
Peleg, N., Blumensaat, F., Molnar, P., Fatichi, S., Burlando, P., 2017. Partitioning the impacts of spatial and climatological rainfall variability in urban drainage modeling. Hydrol. Earth Syst. Sci. 21, 1559–1572.
Prodanovic, P., Simonovic, S.P., 2004. Generation of Synthetic Design Storms for the Upper Thames River Basin. The University of Western Ontario, Department of Civil and Environmental Engineering (Technical Report No. 49).
Rendon, S., Vieux, B., Pathak, C., 2013. Continuous forecasting and evaluation of derived Z-R relationships in a sparse rain gauge network using NEXRAD. J. Hydrol. Eng. 18, 175–182.
Řezáčová, D., Kašpar, M., Müller, M., Sokol, Z., Kakos, V., Hanslian, D., Pešice, P., 2005. A comparison of the flood precipitation episode in August 2002 with historic extreme precipitation events on the Czech territory. Atmos. Res. 77, 354–366.
Rulfová, Z., Kyselý, J., 2013. Disaggregating convective and stratiform precipitation from station weather data. Atmos. Res. 134, 100–115.
Rulfová, Z., Buishand, A., Roth, M., Kyselý, J., 2016. A two-component generalized extreme value distribution for precipitation frequency analysis. J. Hydrol. 534, 659–668.
Šálek, M., Štěpánek, P., Zahradníček, P., 2012. Analysis of rainfall intensities using very dense network measurements and radar information for the Brno area during the period 2003–2009. Meteorol. Z. 21, 29–35.
Schiro, K.A., Neelin, J.D., 2018. Tropical continental downdraft characteristics: mesoscale systems versus unorganized convection. Atmos. Chem. Phys. 18, 1997–2010.
Sokol, Z., 2003. The use of radar and gauge measurements to estimate areal precipitation for several Czech river basins. Stud. Geophys. Geod. 47, 587–604.
Sokol, Z., Bližňák, V., 2009. Areal distribution and precipitation–altitude relationship of heavy short-term precipitation in the Czech Republic in the warm part of the year. Atmos. Res. 94, 652–662.
Sokol, Z., Skripniková, K., Zacharov, P., 2014. Simulation of the storm on 15 August, 2010, using a high resolution COSMO NWP model. Atmos. Res. 137, 100–111.
Štekl, J., Brázdil, R., Kakos, V., Jež, J., Tolasz, R., Sokol, Z., 2001. Extreme Daily Precipitation on the Territory of the Czech Republic in the Period 1879–2000 and their Synoptic Causes. Czech Hydrometeorological Institute, Prague (in Czech).
Thorndahl, S., Einfalt, T., Willems, P., Nielsen, J.E., Veldhuis, M.-C., Arnbjerg-Nielsen, K., Rasmussen, M.R., Molnar, P., 2017. Weather radar rainfall data in urban hydrology. Hydrol. Earth Syst. Sci. 21, 1359–1380.
Tolasz, R., Míková, T., Valeriánová, A., Voženílek, V. (Eds.), 2007. Climate Atlas of Czechia. Czech Hydrometeorological Institute and Palacký University, Prague and Olomouc (256 pp).
Villarini, G., Seo, B.C., Serinaldi, F., Krajewski, W.F., 2014. Spatial and temporal modeling of radar rainfall uncertainties. Atmos. Res. 135-136, 91–101.
Wilks, D.S., 2011. Statistical Methods in the Atmospheric Sciences. Academic Press, New York.
Zhang, J., Howard, K., Langston, C., Kaney, B., Qi, Y., Tang, L., Grams, H., Wang, Y., Cocks, S., Martinaitis, S., Arthur, A., Cooper, K., Brogden, J., Kitzmiller, D., 2016. Multi-radar multi-sensor (MRMS) quantitative precipitation estimation: Initial operating capabilities. Bull. Am. Meteorol. Soc. 97, 621–638.